# Impact of the New South Wales fires during October 2013 on regional air quality in eastern Australia

Géraldine Rea, Clare Paton-Walsh, Solène Turquety, Martin Cope, David Griffith

# Impact of the New South Wales Fires during October 2013 on regional air quality in eastern Australia

Géraldine Rea[a,*], Clare Paton-Walsh[b], Solène Turquety[a], Martin Cope[c], David Griffith[b]

[a] *Laboratoire de Météorologie Dynamique, UMR CNRS 8539, Université Pierre et Marie Curie - Paris 6, Ecole Polytechnique, Palaiseau, France*
[b] *School of Chemistry, University of Wollongong, Wollongong, NSW 2522, Australia*
[c] *CSIRO Marine and Atmospheric Research, Aspendale, VIC 3125, Australia*

**Abstract**

Smoke plumes from fires contain atmospheric pollutants that can be transported to populated areas and effect regional air quality. In this paper, the characteristics and impact of the fire plumes from a major fire event that occurred in October 2013 (17-26) in the New South Wales (NSW) in Australia, near the populated areas of Sydney and Wollongong, are studied. Measurements from the Fourier Transform InfraRed (FTIR) spectrometer located at the University of Wollongong allowed a calculation of specific emission factors (EFs) in terms of grams per kilogram of dry fuel burned: 1640 g $kg^{-1}$ of carbon dioxide; 107 g $kg^{-1}$ of carbon monoxide; 7.8 g $kg^{-1}$ of methane; and 0.16 g $kg^{-1}$ of nitrous oxide. These EFs have then been used to calculate daily fire emissions for the NSW fire event using the APIFLAME emissions' model, leading to an increase of 54% of CO emitted compared to calculations with EFs from Akagi et al. (2011), widely used in the literature.

Simulations have been conducted for this event using the regional chemistry-transport model (CTM) CHIMERE, allowing the first evaluation of its regional impact. Fire emissions are assumed well mixed into the boundary layer. The model simulations have been evaluated compared to measurements at the NSW air quality stations. The mean correlation coefficients (R) are 0.44 for $PM_{10}$, 0.60 for $PM_{2.5}$ and 0.79 for CO, with a negative bias for CO (-14%) and a positive bias for $PM_{2.5}$ (64%). The model shows higher performance for lower boundary layer heights and wind speeds. According to the observations, 7 days show concentrations exceeding the air quality Australian national standards for $PM_{10}$, 8 days for $PM_{2.5}$. In the simulations, 5 days are correctly simulated for $PM_{10}$, 8 days for $PM_{2.5}$. For $PM_{10}$, the model predicts 1 additional day of exceedance (one false detection). During this fire episode, inner Sydney is affected during 5 days by PM exceedances, that are mainly attributed to organic carbon in the model simulations.

To evaluate the influence of the diurnal variability and the injection heights of fire emissions, two additional simulations were performed: one with all fire emissions injected below 1 km (CHIM_1km), since satellite observations suggest low injection for this fire case, and one with a diurnal profile (CHIM_diu) adjusted to best match surface observations closest to the fires. CHIM_1km displays less bias and root mean square error, and CHIM_diu presents a good agreement for hourly statistics for stations where peaks of PM are well captured, but enhances the differences when a peak is overestimated by the model. This sensitivity analysis highlights significant uncertainties related to these two key fire parameters (which add up to uncertainties on emissions), resulting in variations on concentrations of PM and CO.

## 1. Introduction

Emissions from fires have a significant influence on atmospheric composition, due to the quantity of trace gases and aerosols injected during combustion (e.g. Andreae and Merlet, 2001). These emissions can impact locally, regionally and globally the air quality, the radiative budget and the meteorology (Bowman et al., 2009; Langmann et al., 2009; IPCC, 2013). In Australia, bushfires are well known natural hazards, with 54 Mha burned each year on average since 1997 (Giglio et al., 2010). Less well known is that the death toll from air quality impacts may exceed those killed directly in the fires (Johnston et al., 2011, 2013). Fires are more commons in the north , where the tropical savanna is affected every year by fires, but the southeast, where there is the majority of the population (7,3 millions inhabitants in New South Wales), is also regularly affected by extreme fire events (Gupta et al., 2007; Paton-Walsh et al., 2010; Dirksen et al., 2009). During the bushfire seasons (October-February) of 1993-94 and 2002-03 for instance, more than 2,200,000 ha were burned. Moreover, australian bushfires are predicted to increase with higher temperatures as a consequence of climate change, with an increase of 25% of the fire risk in New South Wales (Pitman et al., 2007).

Among many pollutants released in smoke plumes from

*Corresponding author
*Email address:* geraldine.rea@lmd.polytechnique.fr (Géraldine Rea)

fires, fine particles as $PM_{10}$ and $PM_{2.5}$ (particles with an aerodynamical diameter smaller than 10 $\mu$m and 2.5 $\mu$m respectively) can penetrate deeply into the respiratory system and provoke higher risks of mortality and morbidity (Pope III and Dockery, 2006; Johnston et al., 2012). In this context, the World Health Organisation guidelines (followed by the air quality standards from the National Environment Protection Measure (NEPM) of Australia) has set to 50 $\mu$g m$^{-3}$ and 25 $\mu$g m$^{-3}$ the daily mean maximum concentration of respectively $PM_{10}$ and $PM_{2.5}$. From 1994 to 2007 in Sydney, 59% to 90% of PM exceedances were due to fires (Johnston et al., 2011). The precise estimation of atmospheric composition in terms of key pollutants resulting from those fires is thus essential to analyse their air quality impact. For this purpose, numerical simulations by chemistry-transport models (CTM), providing 3-dimensional distributions varying with time, are used.

Fire emissions are accounted for using inventories provided on regional or global scales (van der Werf et al., 2006; Wiedinmyer et al., 2011; Mieville et al., 2010; Turquety et al., 2014). However, uncertainty on these emissions remains high, estimated to up to a factor of 5 for total carbon release, due to different methodologies and uncertainties on burned area products or emission factors (Schultz et al., 2008). Other studies have pointed out the uncertainty associated with the use of daily emissions computed with polar-orbiting satellite fire products (Wang et al., 2006; Sessions et al., 2011). Another key input for modeling fires is the injection height, which has an impact on the fire plume transport and chemistry (Sessions et al., 2011; Paugam et al., 2015).

Modelling fires in Australia are often conducted with global CTMs, i.e at low resolution, and for long range transport (Dirksen et al., 2009) or emissions calculation purposes (Paton-Walsh et al., 2010). In an epidemiological study, Johnston et al. (2012) use a global CTM associated with satellite observations to estimate global PM exposure to smoke from fires. Although many fire regional studies with CTM have been undertaken in other populated areas of the world (for instance Hodzic et al. (2007); Konovalov et al. (2011) in Europe), there are few in Australia and more particularly in the Sydney region. However, air quality monitoring needs finer resolutions than global models.

The purpose of this study is to evaluate air quality impairment by a major bushfire event in Australia, more particularly in New South Wales, using regional chemistry and transport simulations. Therefore, an analysis of the main fire characteristics (*i.e.* area burned, type of vegetation, emission factors), the resulting emissions and the pollution plume simulated is conducted.

The New South Wales (NSW) bushfires during October 2013 were a series of wildfires that burned in rural NSW and brought thick smoke plumes over population centres in Sydney (4.3 millions inhabitants) and Wollongong (290,000 inhabitants). The fires followed the warmest September on record for New South Wales, according to the Australian Bureau of Meteorology, with a daily mean temperature of 19.1°C at Sydney (3.6 °C above the average). The first of the fires started around the 13th October, but serious fires broke out in the Greater Blue Mountains Area to the west of Sydney on the 17th October and 18th October and were largely extinguished by 28th October 2013 (these fires have been detected by satellite and rain radars observations, see Figure 1a and 1b). During this time, high fuel loads and hot, dry and windy conditions led to large fires with a total burned area of 118 thousand hectares (i.e. more than 15% of the total burned for the year 2013), two fatalities and 248 properties lost. Two of the most significant fires during this time were the State Mine fire, which started during explosives training in a military area near Marrangaroo on the 16th October 2013 (the dense aerosol plume was precisely detected by the Australian Bureau of Meteorology rain radar as seen on Figure 1b), and the Hall Road fire, which was ignited by power-lines near Balmoral in the Southern Highlands.

The State Mine fire grew into a major fire by 17th October and the smoke plume from this fire blanketed the densely populated Sydney metropolitan area on the afternoon of the 17th October causing poor air quality including highly elevated $PM_{10}$ values. An estimated area of 56,500 hectares was burnt.

The Hall Road fire broke containment lines on 17th October and the resulting smoke plume extended over large parts of the Illawarra region, including Wollongong (about 35 km from this fire) (see Figure 1). Wollongong was impacted by the fires again in the early hours of 19th October, when a temperature inversion trapped smoke plumes close to the ground for several hours, resulting in peak concentrations of carbon monoxide (CO) in excess of 4 ppm (CO average levels of 124.5 ppb according to Buchholz et al. (submitted)). By the time the Hall Road fire was extinguished, the New South Wales Rural Fire Service estimated that over 15,600 hectares had been burnt.

In this paper, the impact on air quality of this series of bushfires in October 2013 in the Australian New South Wales is studied using a combination of in situ observations and chemistry-transport modeling. We first present the available measurements of the smoke pollution over the region of Sydney and Wollongong, as well as the emission factors derived using a trace gas analyser based on Fourier transform spectroscopy. These measured concentrations of key pollutants are then compared to those predicted by the regional chemistry-transport model CHIMERE, with a focus on air quality reduction.

## 2. Measurements of the chemical composition of smoke from the NSW fires of 2013

The different observations used in this study are described in this section.

### *2.1. Measurements from the University of Wollongong*

The Fourier transform infrared (FTIR) spectrometer located at the University of Wollongong measures carbon

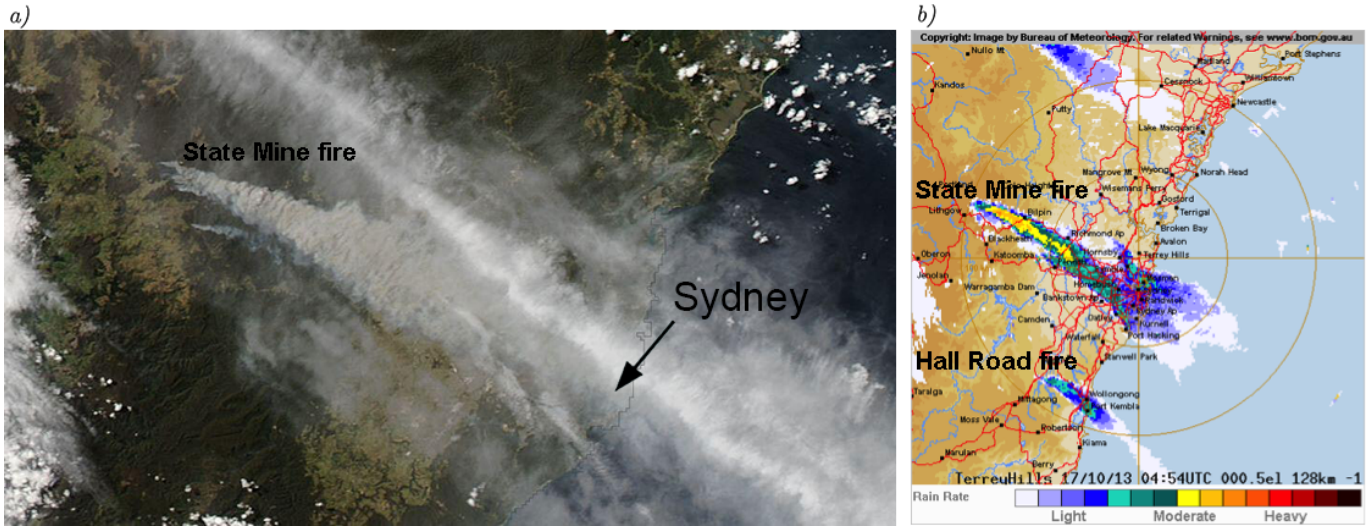


Figure 1: *a) Satellite image courtesy of MODIS Rapide Response Project (NASA/GSFC) with a view of the Blue Mountains fires and the Sydney metropolitan area on 17 October. b) is compiled from the Australian Bureau of Meteorology rain radar at Wollongong for the same day (http://www.bom.gov.au/australia/radar/). The expend and severity of the aerosol plumes is clearly indicated by the radar.*

dioxide ($CO_2$), methane ($CH_4$), carbon monoxide (CO) and nitrous oxide ($N_2O$) in air. The measurements meet the precision and accuracy requirements for World Meteorological Organisation - Global Atmosphere Watch standards for baseline air (Griffith et al., 2012). In Buchholz et al. (submitted), average concentrations between April 2011 and August 2014 have been evaluated to 401.8 ppm for $CO_2$, 1887 ppb for $CH_4$ and 124.5 ppb for CO.

The time-series of CO, $N_2O$, $CH_4$ and $CO_2$ measured using the FTIR spectrometer at Wollongong from late on the 18th October to midnight on the 23rd October 2013 are shown in Figure 2. The pollution caused by the NSW 2013 bushfires is most evident in the CO time-series, which peaks during the early hours of the 19th October 2013, with concentrations of CO above 4 ppm for more than an hour. Strong simultaneous enhancements are also found at this time in $CO_2$, $N_2O$ and $CH_4$. Large night-time enhancements of $CH_4$ occur quite regularly at Wollongong, due to the combination of local sources of $CH_4$ from nearby mining activities and commonplace night-time inversion layers. In fact there is clear indication of such an enhancement in $CH_4$ (see Figure 2) in the form of two large $CH_4$ peaks late on the 18th October and again in the first hours of 19th October 2013. These peaks exceed the $CH_4$ peak that is coincident with the CO peak and indicates potentially mixing of high $CH_4$ air with the air carrying smoke pollution from the fires.

Other pollution events associated with the fires are observed in the CO record shown in Figure 2. On the 20th October CO concentrations were above 500 ppb for 4 hours from 4am to 8am, with peak concentrations exceeding 1 ppm of CO for approximately 15 minutes around 6am. On October 21st CO reached 400 ppb before 1am and remained above this concentration until after 2pm, with concentrations peaking above 1 ppm from 05:35 to after 07:15.

### *2.2. Measurements from the New South Wales air quality monitoring network: Air quality in inner Sydney during fires*

In order to study the regional influence of fires in the full region, we use observations from the New South Wales air quality monitoring network. 41 sites across NSW are maintained by the Office Environment and Heritage (OEH) and provide concentrations of pollutants, with different suites of measurements for each site. Figure 3 shows the location of the stations near Sydney, and the location of the major fire events (Hall Road fire located 30 km from Wollongong and State Mine fire), as well as the winds patterns during the event. Figure 4 shows the time series for CO and $PM_{10}$ at a station located in Sydney-East within the urban environment (Chullora), and at Campbelltown West (Figure 3). These two stations measure CO, $PM_{10}$ and $PM_{2.5}$ at the same time and are within populated areas. Influences of fires are clearly seen, where the daily mean level of pollution for CO is a factor of two higher than long-term daily mean from 16 to 28 October (200 ppb the 15th and up to 600 the 21st according to figure 4).

Fires located to the north west of Sydney are present continuously from 17 to 27 October and reach Sydney with PM and CO peak values on the 17-18th and 21st in the observations. On the 18 and 19 October, fires are additionally detected to the south of Sydney at Wollongong and surrounding stations, in agreement with the measurements from the University of Wollongong described previously. During these episodes, pollutants strongly impact the air quality in the area.

From the concentrations measured at the OEH stations, no exceedances are reported for CO (the maximum concentration allowed is 9 ppm in 8 hours averaging). For particulate matter however, air quality standards are exceeded on many days. Figure 5 shows the time series of the number of stations where an exceedance is detected for $PM_{10}$ (from 19 stations) and $PM_{2.5}$ (from 7 stations) by day, the number for the observations at the OEH stations is represented in black bars. There are 7 days with a daily mean concentration of $PM_{10}$ exceeding the Australian air quality standard of 50 $\mu$g m$^{-3}$, and 9 days with a daily mean concentration of $PM_{2.5}$ exceeding 25 $\mu$g m$^{-3}$, from 16 to 30 October 2013. The most significant number of exceedances of the smoke plumes regarding air quality standards is seen on the 20 and 21, where a large majority of the stations measured an exceedance, corresponding to the most severe fire day.

## 3. Modeling the influence of fires on air quality

### *3.1. The CHIMERE model*

The version 2014b (Menut et al., 2013) of the regional CTM CHIMERE is used. It is driven by meteorological fields computed with the WRF model version 3.5.1 (Skamarock et al., 2008) including nudging above the boundary layer from NCEP global meteorological analysis data (Kalnay et al., 1996). These fields are provided on a regular 1.125° × 1.125° grid.

The boundary conditions for aerosols and trace gases are from simulations by the global model LMDZ-INCA (Folberth et al., 2006), and from GOCART (Ginoux et al., 2001) for dust. The simulations are undertaken using the reduced chemical mechanism MELCHIOR2 which includes 44 species and 120 reactions (a complete list of species and reactions is provided in (Menut et al., 2013)). The aerosol module (Bessagnet et al., 2004) allows the simulation of primary particulate matter and secondary species, with the size distribution simulated using a sectional representation.

The simulations are conducted for three nested domains, represented in Figure 6. The Australian domain is the largest and has a 90 km resolution; it was chosen to ensure all the most important remote sources were captured, which can impact air quality in the smaller domains (e.g. fires from Indonesia, sea salts from south of Australia). The second and third domains are the South East Australian domain, with 27 km of resolution, and the Greater Sydney Region with 9 km of resolution. The vertical discretization is 18 uneven levels, from the surface up to 200 hPa. Chemical concentration output fields are provided at 1 hour time intervals.

Anthropogenic emissions from the Emissions Database for Global Atmospheric Research (EDGAR) prepared for the Hemispheric Transport of Air Pollution (HTAP) program are used. The HTAP-v2 database provides global 0.1° × 0.1° annual emissions for $CH_4$, NMVOC, CO, $SO_2$, NOx, $NH_3$, $PM_{10}$, $PM_{2.5}$, BC and OC and for 7 source sectors, depending on the species (air, ships, energy, industry, transport, residential, agriculture). These are disaggregated into hourly model species and mapped onto the speciated model grid by applying seasonal, daily and weekly factors depending on the source sectors.

Biogenic emissions fluxes are calculated using the global Model of Emissions of Gases and Aerosols from Nature (MEGAN, Guenther et al., 2006) and effect six CHIMERE species (isoprene, $\alpha$-pinene, $\beta$-pinene, limonene, ocimene and NO). MEGAN is based on canopy-scale emission factors depending on the species. Dust emissions are calculated using the (Marticorena and Bergametti, 1995) parametrisation for saltation and the optimized dust production model (Alfaro and Gomes, 2001; Menut et al., 2005) for sandblasting. The dust production model is presented in (Menut et al., 2013) and (Briant et al., 2014), and it is adaptable in different regions. However, it was primarily developed for Africa and Europe and has not been specifically evaluated over Australia.

### *3.2. Fire emissions*

Daily fire emissions were calculated using the APIFLAME fire emissions' model v1.0 (Turquety et al., 2014). APIFLAME calculates carbon emissions by multiplying the area burned with the fuel available for burning specific to the vegetation type burned, and then derives trace gas and aerosol emissions using vegetation-dependant emission factors.

Here, the area burned was estimated using the MODIS active fire detection at 1km resolution (MOD14, Giglio et al. (2010)). Only the fraction of each MODIS pixel covered by vegetation is allowed to burn, as described in Turquety et al. (2014). Figure 7 shows the daily area burned over the NSW region during October 2013 estimated using this MODIS product, and reported by the NSW Rural Fire Service (RFS)[1]. The two data sets present a similar temporal variability, with the higher peaks on the same day (17th of October), although area burnt from RFS is higher by almost a factor of 2 for this day. In total, RFS reported a total area burnt of 1432.52 km$^2$, whereas the total derived from the MODIS hotspots is 1486.05 km$^2$ (almost 5% higher). This difference is relatively small considering the large uncertainty on all parameters involved in the calculation of fire emissions (estimated to ∼100% by Turquety et al. (2014)). We can thus consider that the MODIS dataset is a consistent input for the calculation of the fire emissions in this case, even if the uncertainty concerning the amplitude on the 17th must be taken in consideration in the next results.

For each detected fire, the vegetation is attributed using the MODIS MCD12Q1 collection 5 land cover type product (Friedl et al., 2010). The fraction of vegetation cover burned during the fire episode is shown on Figure

[1] http://www.rfs.nsw.gov.au/

8. The main types of vegetation burned, according to this product, are savanna (65% in mean) and forest (33%). The default classification in the MODIS landcover is not adapted to the NSW specific vegetation types. The combination of savanna and forest in MODIS corresponds to low density forest, woodland and pasture.

The fuel load is derived from simulations output from the ORCHIDEE carbon cycle and vegetation model (Krinner et al., 2005; Maignan et al., 2011), allowing the calculation of carbon emissions. In the NSW region, the average fuel load for savanna is estimated to 6.99 kg $m^{-2}$, and for forests 5.56 kg $m^{-2}$. For savanna, it is greater than the one reported by (Hoelzemann et al., 2004) (1.3 kg $m^{-2}$ for wooded savanna). Finally, APIFLAME uses emission factors taken from (Akagi et al., 2011) and modified for this study, as described in section 4.

Although APIFLAME was initially designed and evaluated for the Euro-Mediterranean region (Turquety et al., 2014), it uses global datasets (described above) and can thus be applied to any region. An ensemble analysis over the Euro-Mediterranean region showed that uncertainty on daily carbon emissions is close to 100%, with a dominant contribution from the area burned and the vegetation map used. Compared to other widely used emission inventories (GFED Mu et al. (2011), GFAS Kaiser et al. (2012)), APIFLAME shows good correlations but discrepancies up to a factor of 2-4 higher in the amplitudes of the emissions. One of the main aims of this paper is to discuss other sources of uncertainties that can effect regional modelling with a state-of-the-art inventory.

Total emissions of CO from fires are shown on Figure 9. Comparing to CO anthropogenic emissions, CO fire emissions are more important for this period (almost a factor of 20), as well as organic carbon, black carbon and other primary organic matter emissions (Table 1). The spatial distribution of fire emissions follows the main events described above. The maximum of the fluxes, in the State Mine Fire, is found to be where forest is in higher proportion than savanna (almost 90%).

Table 1: *Total amount of CO, Organic Carbon (OC), Black Carbon (BC) and other Primary Organic Matter (POM) according to the fire emission inventory APIFLAME, and the anthropogenic inventory EDGAR-HTAP.*

| Species | Anthropogenic $10^{-6}$kg | Fire $10^{-6}$kg |
|---|---|---|
| CO | 28.35 | 529.47 |
| OC | 0.32 | 64.39 |
| BC | 0.23 | 2.48 |
| POM | 1.29 | 49.51 |

### *3.3. Injection heights*

In addition to the total mass emitted, the smoke's injection height is a critical parameter for the modeling of these events. The energy released by these intense events may trigger or reinforce convection (so-called *pyro-convection*). A fraction of the emissions may then be injected directly in the free troposphere, or even in the stratosphere for the most extreme cases. This will strongly impact the concentration at the surface close to the burning regions, but also the long-range transport of the fire plume. Precedent studies concerning injection heights in Australia are rare, but showed some occurrence of plumes reaching the stratosphere in southeastern Australia (Fromm et al., 2006; Dirksen et al., 2009). The analysis of Mims et al. (2010) on grassland fires plumes in central and western Australia with MISR shows that most of the plumes stay concentrated in the near-surface boundary layer, although some can rise higher.

Figure 10 shows the plume heights from the MISR level 2 MIL2TCSP product (Kahn et al., 2007), providing heights of aerosol plumes and clouds. The distribution of the heights from MISR for this specific day (20th October) is shown on Figure 11. Although only one day of measurement is available from MISR for the NSW fires, it suggests that fires were injected at relatively low altitudes (685 m in average above fires, with a maximum at 2830 m).

In CHIMERE, the default parameterization injects emissions throughout the planetary boundary layer (PBL). The simulated PBL heights at the same time as MISR overpass is also shown on Figure 10. The PBL height is consistent with MISR maximum heights, but is higher over the area of the fire plume (1630 m on average above fires at the same time as the MISR overpass, with a maximum at 2440 m). The simulated PBL heights reach more than 4 km in the following hours.

Sensitivity of the simulations to the chosen injection heights will be described in the following section.

### *3.4. Simulations performed*

In this paper, we want to evaluate if the model in its initial configuration, with the additional information on the real emitted quantities, can correctly simulate the air quality impacts of the fires. But other uncertainties that can effect the simulation are also analysed. For this purpose, four simulations have been computed during the time period, restricted to the Sydney region domain. The first one is referred to as the "reference" simulation (CHIM_ref), with daily resolution emissions and emissions injected homogeneously onto the boundary layer. The second simulation is performed using a diurnal profile applied to fire emissions (CHIM_diu). The diurnal profile is chosen as a Gaussian distribution. Although Giglio (2007) and Chédin et al. (2008) showed that the peak of fire activity happened in the late afternoon, surface observations here suggests that the maximum of concentrations is around 1pm, following the winds patterns. We thus choose to put the mean of the Gaussian distribution at this time. The third simulation is computed with fire emissions injected homogeneously under 1 km above the surface (CHIM_1km), to

look at the influence of the injection heights parameter. Finally, a simulation without fires has also been computed to look at the effective influence of the fires.

## 4. Emission factors calculation

Initially, emission factors in APIFLAME are from Akagi et al. (2011), but some adjustments have been made for this study, using the available measurements and following the work of Paton-Walsh et al. (2014) and Smith et al. (2014). Updated values are used for savanna and temperate forest fires in Australia for $CO_2$, CO, $CH_4$, $C_2H_2$, $C_2H_4$, $C_2H_6$, HCHO, $CH_3OH$, $H_3COOH$, HCN and $NH_3$.

As analyzed in section 2.1, the most significant smoke pollution event recorded at the University of Wollongong is on the 19th October. The FTIR spectrometer measures the main carbonaceous species emitted by biomass burning, (90-95% is in the form of $CO_2$ and CO, with the remaining as $CH_4$ or other volatile organic carbon compounds and particulate matter (Akagi et al., 2011)). This means that the measurements may be used to calculate emission factors from the fires, following the method previously used by (Ward and Radke, 1993) :

$$EF_i = F_c \; 1000 \; \frac{MM_i}{12} \; \frac{C_i}{C_T}$$

where $EF_i$ is the mass in grams of species i emitted per kilogram of dry fuel consumed, (g $kg^{-1}$); $F_c$ is the fractional carbon content of the fuel (assumed here to be $0.50 \pm 0.05$ for all hazard reduction burns (Yokelson et al., 1999)); $MM_i$ is the molecular mass of species i and 12 is the atomic mass of carbon; $C_i/C_T$ is the number of moles of species i emitted divided by the total number of moles of carbon emitted, and may be calculated using emission ratios with respect to a reference species (usually $CO_2$) via equations 2:

$$\frac{C_i}{C_T} = \frac{ER(i/CO_2)}{\sum_{j=1}^{n}(NC_j \; ER(j/CO_2))}$$

The emission ratios (or enhancement ratios[2]) may be determined from the gradient of the linear best fit to a plot of the abundance of species i against the abundance of reference species $CO_2$, thereby removing the requirement for accurate knowledge of the background mole fractions. Use of only $CO_2$, CO and $CH_4$ in this mass balance equation has been estimated to artificially inflate the emission factors by 1-2% (Yokelson et al., 2007).

Using only data from 19th October from 03:00 to 07:45 (in an attempt to avoid the interference from other sources of $CH_4$ enhancements), we determined the following enhancement ratios to $CO_2$: $CO/CO_2 = 0.102$ ($R^2$=0.96); $CH_4/CO_2 = 0.013$ ($R^2$=0.94) and $N_2O/CO_2 = 0.000095$ ($R^2$ =0.98). These enhancement ratios are equivalent to 89.7% of the emitted carbon detected as $CO_2$, 9.1% as CO and 1.2% as $CH_4$ and yield a modified combustion efficiency (Hao and Ward, 1993) for the fires of 0.91.

Emission factors for the fires calculated from these measurements (in grams of gas emitted per kilogram of dry fuel burned) are 1640 g $kg^{-1}$ of carbon dioxide; 107 g $kg^{-1}$ of carbon monoxide; 7.8 g $kg^{-1}$ of methane; and 0.16 g $kg^{-1}$ of nitrous oxide. The values calculated in this study are consistent with emission factors measured at controlled burns in New South Wales of $1620 \pm 160$ g $kg^{-1}$ of carbon dioxide; $120 \pm 20$ g $kg^{-1}$ of carbon monoxide; $3.6 \pm 1.1$ g $kg^{-1}$ of methane; and $0.15 \pm 0.09$ g $kg^{-1}$ of nitrous oxide (Paton-Walsh et al., 2014).

Thus the results are in good agreement with previous emission factors measured from this ecosystem, except for the emission factor calculated here for $CH_4$. The much larger emission factor determined for $CH_4$ could indicate residual interference from alternative sources of $CH_4$, as described above, or possibly result from direct influence from the State Mine fire, which could emit more $CH_4$ than a typical fire.

These emission factors are used in the simulation of the fires, for the APIFLAME inventory. With those factors, the total mass of CO emitted for the fires during October 2013 is 0.33 Tg, whereas it is 0.22 Tg with the initial emission factors from Akagi et al. (2011), i.e. 54% more CO released. Considering this difference, uncertainties have to be considered on other pollutants whose EF have not been modified, such as particulate matter, on the following results.

## 5. Comparison of simulations to measurements

Figure 6 shows the mean concentration of $PM_{2.5}$ and CO over the Australian domain from 16 to 28 October obtained with the CHIMERE simulation. The fire episode in NSW is clearly seen, with mean concentrations of $PM_{2.5}$ up to 60 $\mu$g $m^{-3}$. Organic carbon is the dominating contributor to $PM_{2.5}$ with primary organic matter (not shown), and the fire plume is transported to the south over the Tasman sea. Note that the strong $PM_{2.5}$ levels around $-50°$ in CHIMERE are due to sea salt (with a contribution up to 20 $\mu$g $m^{-3}$).

Modeled surface concentrations in the Sydney region domain during the fire period are compared with measurements from the OEH stations (described in Section 2.2) for PM and CO. A comparison is also done with the results of the FTIR spectrometer (Section 2.1) for CO. This paper is focused on particulate matter' impacts on air quality, but CO, as a signature of fires, is also evaluated in this section.

Modeled (CHIM_ref) and observed daily mean and max concentrations for CO and PM at OEH stations are shown

[2]Note that when the measurements are made downwind of the fire in aged smoke, then these same ratios are commonly referred to as "enhancement ratios", to highlight the fact that chemical and physical processing may have altered the ratio of species from that which was originally emitted from the fire (this adds additional uncertainty to the emission factors calculated from these measurements, compared to similar measurements made close to the fires).

on Figure 12. The simulation shows high levels of pollution close to fire sources, but decreasing rapidly as the distance from the fire increases, in good agreement with the observations, the majority of which are located at some distance from the fires (minimum 30 km). Concentrations of CO reached up to 2.5 ppm at the source according to the model, but only reach 1.5 ppm near urban areas. However, the stations measured high values (above 1.7 ppm at two stations). For particulate matter, the concentration close to the fires are also very high according to CHIMERE, reaching more than 600 $\mu$g m$^{-3}$ for fine particles. At the stations, the 1-hour mean levels are under 50 $\mu$g m$^{-3}$ with a maximum up to 350 $\mu$g m$^{-3}$ for $PM_{2.5}$. The spatial patterns shows good agreement with the locations of the fire, with the most important being the State Mine fire as described above.

### *5.1. Simulation of the fires' impact on air quality*

Air quality impact was evaluated by analyzing the number of threshold exceedances.

Table 2 shows the number of exceedances detected at each station for observed and modeled concentrations. These exceedances are also plotted on Figure 5 for the CHIMERE and the observations during the NSW fire episode. The CHIMERE model assigns all the exceedances of PM to fires.

For $PM_{2.5}$, the number of exceedances detected by the model is overestimated by a factor of 2 (46 versus 22), whereas it is better represented for $PM_{10}$ (94 versus 75). In general the model manages to detect the number of days where an exceedance is observed. For all the stations in Sydney area and Wollongong, 5 days from 7 show $PM_{10}$ exceedances in agreement with observations, 2 days are missed and 1 is only seen by CHIMERE, and 8 days of 10 $PM_{2.5}$ exceedances ares seen by CHIMERE with no false detections.

In total from 16 to 28 October, almost all days had exceedances due to fires in the entire Sydney region grid, with a maximum of 25% of the domain with $PM_{2.5}$ concentration over 25 $\mu$g m$^{-3}$ (and 20% of the domain with $PM_{10}$ concentration over 50 $\mu$g m$^{-3}$) on the 19 October. The majority of exceedances are concentrated over 50 km around the fire sources, and inner Sydney is affected during 5 days with thresholds exceeded. In 2013, exceedences in NSW are relatively rare and mainly result from these fires according to the OEH network.

During these exceedances, $PM_{2.5}$ is composed mainly of organic carbon (53.5%, with 53.2% due to fires), other primary organic matter (23.6%, with 23.1% due to fires), secondary organic aerosols (7.6%, with 5.6% due to fires) and sea salt (7.8%). The composition of $PM_{10}$ during exceedances is similar, with in proportion less organic carbon (45%), more sea salt (9.5%) and slightly more other primary organic matter (33%) and secondary organic aerosols (6.2%).

### *5.2. Evaluation of the fire case*

Table 2 summarizes the statistics over all the stations, for CO, $PM_{10}$ and $PM_{2.5}$ concentrations. Figure 4 shows the time series of pollutants (for the model simulations and the observations), at Chullora and Campbelltown West. The time series of CO from the FTIR spectrometer in Wollongong near the Balmoral fire is also shown on Figure 2 (first plot). The three stations are indicated with arrows in Figure 12.

For $PM_{10}$, with the higher number of stations, correlations ranges from -0.41 (Singleton South) to 0.91 (Kembla Grange). The repartition of the correlation is shown on figure 13. Stations located near Singleton, in the extreme north of the domain are poorly simulated (no or negative correlation associated with high RMSE). The fire that occurred in this area is the weakest and is relatively far from the stations compared to others. Large mines are also present in this area that are not captured by the EDGAR inventory, additionally to a complex topography that need higher spatial resolution.

For the rest of the stations, the correlation between modelled and observed $PM_{10}$ is systematically above 0.5, except at Bargo (0.21). For $PM_{2.5}$ and CO, the comparison shows good correlations (0.60 on average for $PM_{2.5}$, 0.79 for CO). The model tends to overestimate $PM_{2.5}$ (mean bias of 64%) and underestimate CO (-14%). The temporality of daily emissions are thus correctly captured by the model. Moreover, 90% of the $PM_{2.5}$ stations and 75% of the $PM_{10}$ stations meet the performance criteria defined by (Boylan and Russell, 2006) (both the mean fractional bias and the mean fractional error are lower than or equal to 75% and $\pm$60% respectively), suggesting a good performance of the model.

However, although some peaks of concentrations are modelled at the right time, the root mean square error (RMSE) can be high at some stations. This is due to missing concentration peaks or plumes, to some that are not simulated at the right place, or to underestimations of the peaks of concentrations themselves.

For instance, the peak in CO and PM concentrations observed on the 17th of October in Sydney is missed by the model. A significant amount of emissions are however released that day in the model, although underestimated compare to the RFS report (Figure 7), but it is not transported toward Sydney (Figure 15a).

At Wollongong, the 18th is the main day affected by fires (Balmoral fires), and is underestimated by the model (1.5 ppm for CO instead of 4.5 ppm and 380 $\mu$g m$^{-3}$ instead of 570 $\mu$g m$^{-3}$ for PM) but not missed. On that day, RFS reported area burned is also underestimated by our calculation from MODIS (Figure 7), due to less of the vegetation burned attributed to forest and more to savanna on that day in the model. For PM however, the daily mean value is in good agreement with the observations.

On the 18-19 October, levels of PM are correctly simu-

lated by CHIMERE for all the simulations in Sydney (PM up to 100 $\mu$g m$^{-3}$ for both observations and model and 200 $\mu$g m$^{-3}$ at Campbelltown West).

On 21 October, the strongest concentration peak in Sydney is underestimated by CHIM_ref, up to 1 ppm for CO versus 1.5 ppm in the observations, and 200 $\mu$g m$^{-3}$ versus almost 300 $\mu$g m$^{-3}$ for $PM_{10}$. The simulated peak is also more spread over the day than in the observations.

In Campbelltown West however, the peak is missed by CHIMERE. Observations shows concentrations up to 9 ppm for CO and 900 $\mu$g m$^{-3}$ for $PM_{10}$, and although simulations show similar values very close to the fire source, it is not transported to the south (the transport of the plume follows a south-east direction that day) and concentrations rapidly decrease.

Finally, a strong peak of PM and CO concentrations is seen in the model on the 25 October at Sydney stations, but the peak is overestimated by a factor of around 3 compared to CO and PM observations.

To bring some explanation of the reasons why certain peaks of concentrations are correctly simulated and other not, we looked at some meteorology fields during the different events. Figure 14 represents the daily mean of the modelled PBL heights averaged above the fire grid cells only, and Figure 15 the winds on 17 October (peak of concentration missed at the majority of the stations) and 21 October (correct detection of the plume). PBL heights appear to be minimum on the 18-19-20-21 October, corresponding to the time when the concentration peaks are not missed by the model. In addition, the wind speed is lower on these days, as shown on Figure 15 b. On the contrary, the PBL is higher and the winds stronger on the 17 October for instance. The meteorological conditions drives the main transport of the plume, and the peak in concentrations of pollutants are correctly simulated when the plume is not transported far and stays near the source.

### *5.3. Influence of the injection heights and the diurnal variability of the fire emissions*

In this section, we discuss the impact of the key parameters that contribute to the modelling of pollutants released from fires. The results of the different simulations CHIM_1km and CHIM_diu are represented on the time series at the stations Wollongong, Campbelltown West and Chullora (Figures 2 and 4).

The differences between CHIM_ref and CHIM_1km are relatively low. The mixing into the BL is thus relatively quick in the model at the scale of the fire, and the meteorological conditions drive the main transport of the plume. However, the bias of the CHIM_1km is lower, particularly for CO (-9.5% instead of -14%). This can be explained by the punctual peak concentrations, that are more intense (and thus less underestimated) when the emissions are injected near the surface and less diluted on the vertical column.

Applying a diurnal profile to the emissions has a direct impact on hourly concentrations peaks, that are higher than the baseline simulation, increasing hourly correlation coefficients (0.39 to 0.45 for CO, 0.35 to 0.40 for $PM_{2.5}$). Particularly, PM concentrations in Wollongong and Chullora for the 18th and the 21st of October are better simulated with diurnal variability of fire emissions (Figure 4). However, peaks that are only seen by the model are also higher and so that the total bias is not improved.

## 6. Summary and Conclusions

A detailed analysis has been undertaken for the New South Wales bushfires of 2013 that burned in rural New South Wales in October 2013 and produced smoke plumes transported over populated areas in Sydney and Wollongong. To our knowledge, it is the first analysis on these fires in the literature both with a regional model and with observations.

Measurements from the Fourier Transform infrared spectrometer in University of Wollongong allowed the retrieval of concentrations of CO, $CO_2$, $CH_4$ and $N_2O$, determining several characteristics of the studied fires. The calculation of emissions factors from enhancements ratios have been made from these data, and are (in grams of gas emitted per kilogram of dry fuel burned) : 1640 g kg$^{-1}$ of carbon dioxide; 107 g kg$^{-1}$ of carbon monoxide; 7.8 g kg$^{-1}$ of methane; and 0.16 g kg$^{-1}$ of nitrous oxide, although interfering methane sources cause doubt on the emission factor for methane. These values are in agreement (except for methane) with other studies on the main types of vegetation and have been used as an input for the fire inventory used in the chemistry-transport model CHIMERE. Having this type of measurements is precious in the context of the high uncertainties regarding the emission inventories. In this particular case, the amount of CO released is 54% higher in APIFLAME compare to the amount computed with the emission factors from Akagi et al. (2011).

Four simulations have been computed with the CHIMERE model, to evaluate the influence of key parameters. A simulation (CHIM_ref) has been computed with initial parametrization of the model (daily fire emissions from the APIFLAME inventory, and pollutants injected homogeneously into the PBL). Two additional simulations, one with a gaussian diurnal profile for fire emissions (CHIM_diu) and one with pollutants injected below 1 km (CHIM_1km) have also been computed and compared to the observations. Finally, a simulation without fire emissions has also been computed to see the effective influence of the fires in the modelling.

Globally, the levels and the consistent variability of the simulated surface concentrations allows a good overview of the number of days that exceed the air quality standards defined by the NEPM: for $PM_{10}$, 5 days from 7 are detected in agreement with observations, with 2 days missed and 1 false alarm. For $PM_{2.5}$, 8 days of 10 are detected in agreement with observations, with no false detection. A maximum of 20% of the Sydney region domain is affected by $PM_{10}$ exceedances, 25% for $PM_{2.5}$ exceedances, with a

composition mainly of organic carbon (53.5%) and other primary organic matter (23.6%).

The simulated concentrations of CO and particulate matter from CHIMERE have been compared to the stations and the FTIR spectrometer. The model generally captures the variability of the levels of concentrations at 17 stations for $PM_{10}$, with correlation coefficients ranging from 0.53 to 0.92, and does not captures the variability at 7 stations (no correlation or anti-correlated). The performance of the model concerning particulate matter is correct in the majority of the stations, with 90% of the $PM_{2.5}$ stations and 75% of the $PM_{10}$ stations that meet the performance criteria defined by (Boylan and Russell, 2006).

However, the model in its initial configuration underestimates the largest smoke impact in Sydney on 21 October (1 ppm fo CO versus 1.5 ppm, and 200 versus 300 $\mu$g m$^{-3}$ for $PM_{10}$ at the station Chullora), whereas CHIM_diu managed to reproduce the peak, so that diurnal variability for fire emissions improves peak values initially modeled at the right time and location. Results of CHIM_1km are very close to CHIM_ref, but with less bias and RMSE. CHIM_diu does not improve the daily statistics but influence hourly values.

The transport pathway of the fire plume is a source of uncertainty, leading to an inconsistency with the observations for instance on the 21 October in Campbelltown West (where a peak is missing although large fire emissions are released this day). The transport is correctly simulated when the meteorological conditions favors the confinement of the fire emissions closer to the surface (boundary layer and winds lower than average).

This analysis suggests that a regional model is able to reproduce the variability of a fire event despite the existing uncertainties on fire emissions inventories. But predicting the correct amplitude is challenged by various uncertainties: from the magnitude and diurnal variation of the fire emissions and from the transport pathways of the fire plumes, influenced itself by the meteorological conditions which can confine fire emissions closer to the surface. This study suggests that to reduce uncertainties, a particular attention must be paid first concerning the meteorology and particularly the wind patterns and the PBL used. In analysis studies, it may improve results to use analyzed meteorology for instance, but for operational prediction purposes, discrepancies can be large because of this uncertainty.

We also showed on this study that the diurnal variability of fire emissions can lead to large differences between simulations. This suggests that, even if the daily temporal variability of the fire events was captured, a more realistic diurnal variability should be used, which cannot be obtained by polar satellites such as MODIS being used to constrain fire inventories.


## Acknowledgement

We wish to thank financial support for this project from EIT - Climate-KIC. Authors are grateful to the National Aeronautics and Space Agency (NASA) for the availability of the MODIS and MISR data. The Office of Environment and Heritage is thanked for providing data from the NSW air quality monitoring network. The Rural Fire Service is also thanked for the database concerning the reported burned area.


## References


Akagi, S. K., Yokelson, R. J., Wiedinmyer, C., Alvarado, M. J., Reid, J. S., Karl, T., Crounse, J. D., Wennberg, P. O., 2011. Emission factors for open and domestic biomass burning for use in atmospheric models. Atmospheric Chemistry and Physics 11 (9), 4039–4072.

Alfaro, S. C., Gomes, L., 2001. Modeling mineral aerosol production by wind erosion: Emission intensities and aerosol size distributions in source areas. Journal of Geophysical Research: Atmospheres 106 (D16), 18075–18084.

Andreae, M. O., Merlet, P., 2001. Emission of trace gases and aerosols from biomass burning. Global Biogeochemical Cycles 15 (4), 955–966.

Bessagnet, B., Hodzic, A., Vautard, R., Beekmann, M., Cheinet, S., Honoré, C., Liousse, C., Rouil, L., 2004. Aerosol modeling with CHIMERE: preliminary evaluation at the continental scale. Atmospheric Environment 38 (18), 2803–2817.

Bowman, D. M., Balch, J. K., Artaxo, P., Bond, W. J., Carlson, J. M., Cochrane, M. A., D'Antonio, C. M., DeFries, R. S., Doyle, J. C., Harrison, S. P., et al., 2009. Fire in the earth system. science 324 (5926), 481–484.

Boylan, J. W., Russell, A. G., 2006. Pm and light extinction model performance metrics, goals, and criteria for three-dimensional air quality models. Atmospheric Environment 40 (26), 4946–4959.

Briant, R., Menut, L., Siour, G., Prigent, C., 2014. Homogeneized modeling of mineral dust emissions over europe and africa using the CHIMERE model. Geoscientific Model Development Discussions 7 (3), 3441–3480.

Buchholz, R., Paton-Walsh, C., Griffith, D., Kubistin, D., Caldow, C., Fisher, J., Deutscher, N., Kettlewell, G., Riggenbach, M., Macatangay, R., Krummel, P., Langenfelds, R., submitted. Source and meteorological influences on air quality (co, $ch_4$ & $co_2$) at a southern hemisphere urban site. Atmospheric Environment.

Chédin, A., Scott, N. A., Armante, R., Pierangelo, C., Crevoisier, C., Fossé, O., Ciais, P., 2008. A quantitative link between co2 emissions from tropical vegetation fires and the daily tropospheric excess (dte) of $co_2$ seen by noaa-10 (19871991). Journal of Geophysical Research: Atmospheres 113 (D5), d05302.

Dirksen, R. J., Folkert Boersma, K., de Laat, J., Stammes, P., van der Werf, G. R., Val Martin, M., Kelder, H. M., 2009. An aerosol boomerang: Rapid around-the-world transport of smoke from the december 2006 australian forest fires observed from space. Journal of Geophysical Research: Atmospheres 114 (D21).

Folberth, G. A., Hauglustaine, D. A., Lathière, J., Brocheton, F., 2006. Interactive chemistry in the laboratoire de mtorologie dynamique general circulation model: model description and impact analysis of biogenic hydrocarbons on tropospheric chemistry. Atmospheric Chemistry and Physics 6 (8), 2273–2319.

Friedl, M. A., Sulla-Menashe, D., Tan, B., Schneider, A., Ramankutty, N., Sibley, A., Huang, X., 2010. MODIS collection 5 global land cover: Algorithm refinements and characterization of new datasets. Remote Sensing of Environment 114 (1), 168–182.

Fromm, M., Tupper, A., Rosenfeld, D., Servranckx, R., McRae, R., 2006. Violent pyro-convective storm devastates australia's capital and pollutes the stratosphere. Geophysical Research Letters 33 (5), l05815.

Giglio, L., 2007. Characterization of the tropical diurnal fire cycle using virs and modis observations. Remote Sensing of Environment 108 (4), 407–421.

Giglio, L., Randerson, J. T., van der Werf, G. R., Kasibhatla, P. S., Collatz, G. J., Morton, D. C., DeFries, R. S., 2010. Assessing variability and long-term trends in burned area by merging multiple satellite fire products. Biogeosciences 7 (3), 1171–1186.

Ginoux, P., Chin, M., Tegen, I., Prospero, J. M., Holben, B., Dubovik, O., Lin, S.-J., 2001. Sources and distributions of dust aerosols simulated with the gocart model. Journal of Geophysical Research: Atmospheres 106 (D17), 20255–20273.

Griffith, D. W. T., Deutscher, N. M., Caldow, C., Kettlewell, G., Riggenbach, M., Hammer, S., 2012. A fourier transform infrared trace gas and isotope analyser for atmospheric applications. Atmospheric Measurement Techniques 5 (10), 2481–2498.

Guenther, A., Karl, T., Harley, P., Wiedinmyer, C., Palmer, P., Geron, C., 2006. Estimates of global terrestrial isoprene emissions using MEGAN (Model of Emissions of Gases and Aerosols from Nature). Atmos. Chem. Phys. 6, 3181–3210.

Gupta, P., Christopher, S. A., Box, M. A., Box, G. P., 2007. Multi year satellite remote sensing of particulate matter air quality over sydney, australia. International Journal of Remote Sensing 28 (20), 4483–4498.

Hao, W. M., Ward, D. E., 1993. Methane production from global biomass burning. Journal of Geophysical Research: Atmospheres 98 (D11), 20657–20661.

Hodzic, A., Madronich, S., Bohn, B., Massie, S., Menut, L., Wiedinmyer, C., 2007. Wildfire particulate matter in europe during summer 2003: meso-scale modeling of smoke emissions, transport and radiative effects. Atmospheric Chemistry and Physics 7 (15), 4043–4064.

Hoelzemann, J. J., Schultz, M. G., Brasseur, G. P., Granier, C., Simon, M., 2004. Global wildland fire emission model (gwem): Evaluating the use of global area burnt satellite data. Journal of Geophysical Research: Atmospheres 109 (D14).

IPCC, 2013. Climate change 2013: The physical science basis. contribution of working group i to the fifth assessment report of the intergovernmental panel on climate change [stocker, t.f., d. qin, g.-k. plattner, m. tignor, s.k. allen, j. boschung, a. nauels, y. xia, v. bex and p.m. midgley (eds.)].

Johnston, F., Hanigan, I., Henderson, S., Morgan, G., Bowman, D., 2011. Extreme air pollution events from bushfires and dust storms and their association with mortality in sydney, australia 1994-2007. Environmental research 111 (6), 811–816.

Johnston, F. H., Hanigan, I. C., Henderson, S. B., Morgan, G. G., 2013. Evaluation of interventions to reduce air pollution from biomass smoke on mortality in launceston, australia: retrospective analysis of daily mortality, 1994-2007. BMJ 346.

Johnston, F. H., Henderson, S. B., Chen, Y., Randerson, J. T., Marlier, M., DeFries, R. S., Kinney, P., Bowman, D. M., Brauer, M., 2012. Estimated global mortality attributable to smoke from landscape fires. Environmental health perspectives 120 (5).

Kahn, R. A., Garay, M. J., Nelson, D. L., Yau, K. K., Bull, M. A., Gaitley, B. J., Martonchik, J. V., Levy, R. C., 2007. Satellite-derived aerosol optical depth over dark water from MISR and MODIS: Comparisons with AERONET and implications for climatological studies. Journal of Geophysical Research: Atmospheres 112 (D18).

Kaiser, J. W., Heil, A., Andreae, M. O., Benedetti, A., Chubarova, N., Jones, L., Morcrette, J.-J., Razinger, M., Schultz, M. G., Suttie, M., van der Werf, G. R., 2012. Biomass burning emissions estimated with a global fire assimilation system based on observed fire radiative power. Biogeosciences 9 (1), 527–554.

Kalnay, E., Kanamitsu, M., Kistler, R., Collins, W., Deaven, D., Gandin, L., Iredell, M., Saha, S., White, G., Woollen, J., Zhu, Y., Chelliah, M., Ebisuzaki, W., Higgins, W., Janowiak, J., Mo, K., Ropelewski, C., Wang, J., Leetmaa, A., Reynolds, R., Jenne, R., Joseph, D., 1996. The NCEP/NCAR 40-year reanalysis project. Bull. Amer. Meteorol. Soc. 77, 437–471.

Konovalov, I. B., Beekmann, M., Kuznetsova, I. N., Yurova, A., Zvyagintsev, A. M., 2011. Atmospheric impacts of the 2010 russian wildfires: integrating modelling and measurements of an extreme air pollution episode in the moscow region. Atmospheric Chemistry and Physics 11 (19), 10031–10056.

Krinner, G., Viovy, N., de Noblet-Ducoudré, N., Ogée, J., Polcher, J., Friedlingstein, P., Ciais, P., Sitch, S., Prentice, I. C., 2005. A dynamic global vegetation model for studies of the coupled atmosphere-biosphere system. Global Biogeochemical Cycles 19 (1), gB1015.

Langmann, B., Duncan, B., Textor, C., Trentmann, J., van der Werf, G. R., 2009. Vegetation fire emissions and their impact on air pollution and climate. Atmospheric Environment 43 (1), 107–116.

Maignan, F., Bréon, F.-M., Chevallier, F., Viovy, N., Ciais, P., Garrec, C., Trules, J., Mancip, M., 2011. Evaluation of a global vegetation model using time series of satellite vegetation indices. Geoscientific Model Development 4 (4), 1103–1114.

Marticorena, B., Bergametti, G., 1995. Modeling the atmospheric dust cycle: 1. Design of a soil-derived dust emission scheme. Journal of Geophysical Research: Atmospheres 100 (D8), 16415–16430.

Menut, L., Bessagnet, B., Khvorostyanov, D., Beekmann, M., Blond, N., Colette, A., Coll, I., Curci, G., Foret, G., Hodzic, A., Mailler, S., Meleux, F., Monge, J., Pison, I., Siour, G., Turquety, S., Valari, M., Vautard, R., Vivanco, M., 2013. CHIMERE 2013: a model for regional atmospheric composition modelling. Geoscientific Model Development 6, 981–1028.

Menut, L., Schmechtig, C., Marticorena, B., 2005. Sensitivity of the sandblasting fluxes calculations to the soil size distribution accuracy. Journal of Atmospheric and Oceanic Technology 22, 1875–1884.

Mieville, A., Granier, C., Liousse, C., Guillaume, B., Mouillot, F., Lamarque, J., Grégoire, J., Pétron, G., 2010. Emissions of gases and particles from biomass burning during the 20th century using satellite data and an historical reconstruction. Atmospheric Environment 44 (11), 1469–1477.

Mims, S., Kahn, R., Moroney, C., Gaitley, B., Nelson, D., Garay, M., Jan 2010. MISR stereo heights of grassland fire smoke plumes in australia. Geoscience and Remote Sensing, IEEE Transactions on 48 (1), 25–35.

Mu, M., Randerson, J. T., van der Werf, G. R., Giglio, L., Kasibhatla, P., Morton, D., Collatz, G. J., DeFries, R. S., Hyer, E. J., Prins, E. M., Griffith, D. W. T., Wunch, D., Toon, G. C., Sherlock, V., Wennberg, P. O., 2011. Daily and 3-hourly variability in global fire emissions and consequences for atmospheric model predictions of carbon monoxide. Journal of Geophysical Research: Atmospheres 116 (D24), d24303.

Paton-Walsh, C., Emmons, L. K., Wilson, S. R., 2010. Estimated total emissions of trace gases from the canberra wildfires of 2003: a new method using satellite measurements of aerosol optical depth & the mozart chemical transport model. Atmospheric Chemistry and Physics 10 (12), 5739–5748.

Paton-Walsh, C., Smith, T. E. L., Young, E. L., Griffith, D. W. T., Guérette, E.-A., 2014. New emission factors for australian vegetation fires measured using open-path fourier transform infrared spectroscopy - part 1: Methods and australian temperate forest fires. Atmospheric Chemistry and Physics 14 (20), 11313–11333.

Paugam, R., Wooster, M., Freitas, S. R., Val Martin, M., 2015. A review of approaches to estimate wildfire plume injection height within large scale atmospheric chemical transport models part 1. Atmospheric Chemistry and Physics Discussions 15 (6), 9767–9813.

Pitman, A., Narisma, G., McAneney, J., 2007. The impact of climate change on the risk of forest and grassland fires in australia. Climatic Change 84 (3-4), 383–401.

Pope III, C. A., Dockery, D. W., 2006. Health effects of fine particulate air pollution: lines that connect. Journal of the Air & Waste Management Association 56 (6), 709–742.

Schultz, M. G., Heil, A., Hoelzemann, J. J., Spessa, A., Thonicke, K., Goldammer, J. G., Held, A. C., Pereira, J. M. C., van het Bolscher, M., 2008. Global wildland fire emissions from 1960 to 2000. Global Biogeochemical Cycles 22 (2).

Sessions, W. R., Fuelberg, H. E., Kahn, R. A., Winker, D. M., 2011.

An investigation of methods for injecting emissions from boreal wildfires using WRF-Chem during ARCTAS. Atmospheric Chemistry and Physics 11 (12), 5719–5744.

Skamarock, W., Klemp, J., Dudhia, J., Gill, D., Barker, D., Duda, M., Huang, X., Wang, W., Powers, J., 2008. A description of the advanced research WRF version 3. NCAR Technical Note, 123pp.

Smith, T. E. L., Paton-Walsh, C., Meyer, C. P., Cook, G. D., Maier, S. W., Russell-Smith, J., Wooster, M. J., Yates, C. P., 2014. New emission factors for australian vegetation fires measured using open-path fourier transform infrared spectroscopy - part 2: Australian tropical savanna fires. Atmospheric Chemistry and Physics 14 (20), 11335–11352.

Turquety, S., Menut, L., Bessagnet, B., Anav, A., Viovy, N., Maignan, F., Wooster, M., 2014. APIFLAME v1.0: High resolution fire emission model and application to the Euro-Mediterranean region. Geoscientific Model Development 7, 587–612.

van der Werf, G. R., Randerson, J. T., Giglio, L., Collatz, G. J., Kasibhatla, P. S., Arellano Jr., A. F., 2006. Interannual variability in global biomass burning emissions from 1997 to 2004. Atmospheric Chemistry and Physics 6 (11), 3423–3441.

Wang, J., Christopher, S. A., Nair, U. S., Reid, J. S., Prins, E. M., Szykman, J., Hand, J. L., 2006. Mesoscale modeling of central american smoke transport to the united states: 1. top-down assessment of emission strength and diurnal variation impacts. Journal of Geophysical Research: Atmospheres 111 (D5), d05S17.

Ward, D., Radke, L., 1993. Emissions measurements from vegetation fires: A comparative evaluation of methods and results. Fire in the Environment: The Ecological, Atmospheric and Climatic Importance of Vegetation Fires 13, 53–76.

Wiedinmyer, C., Akagi, S. K., Yokelson, R. J., Emmons, L. K., Al-Saadi, J. A., Orlando, J. J., Soja, A. J., 2011. The fire inventory from ncar (finn): a high resolution global model to estimate the emissions from open burning. Geoscientific Model Development 4 (3), 625–641.

Yokelson, R. J., Goode, J. G., Ward, D. E., Susott, R. A., Babbitt, R. E., Wade, D. D., Bertschi, I., Griffith, D. W. T., Hao, W. M., 1999. Emissions of formaldehyde, acetic acid, methanol, and other trace gases from biomass fires in north carolina measured by airborne fourier transform infrared spectroscopy. Journal of Geophysical Research: Atmospheres 104 (D23), 30109–30125.

Yokelson, R. J., Karl, T., Artaxo, P., Blake, D. R., Christian, T. J., Griffith, D. W. T., Guenther, A., Hao, W. M., 2007. The tropical forest and fire emissions experiment: overview and airborne fire emission factor measurements. Atmospheric Chemistry and Physics 7 (19), 5175–5196.

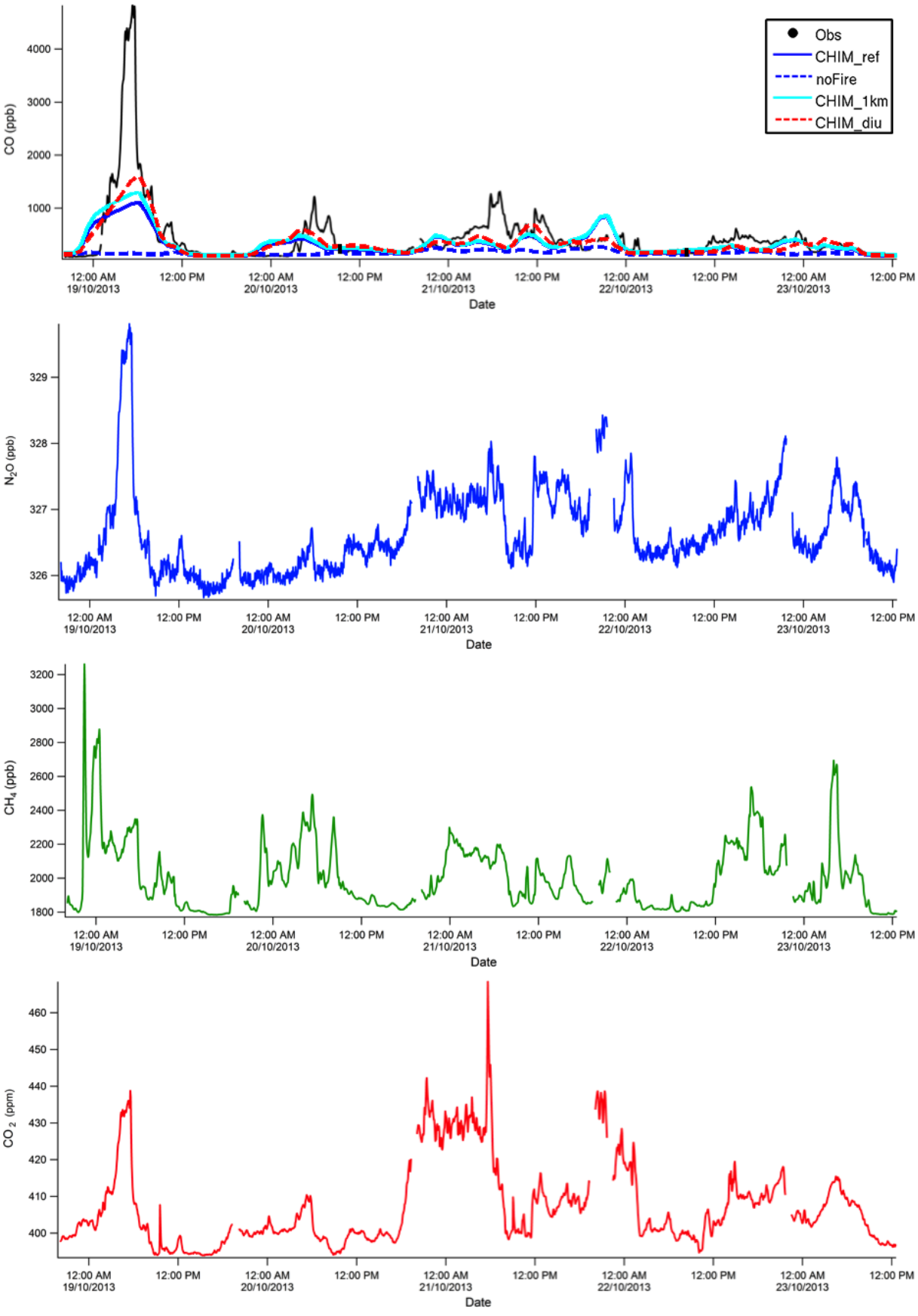


Figure 2: *Time-series of CO, $N_2O$, $CH_4$ and $CO_2$ measured using the FTIR spectrometer at Wollongong during the NSW 2013 bushfires.*

Table 2: *Daily performance statistics for CO and PM concentrations simulated with CHIMERE (Mod.) compared to OEH measurements and the FTIR spectrometer of Wollongong (Obs.) from 16 to 28 October 2013. The number of exceedances corresponds to the number of time that the threshold defined by NEPC is exceeded: 50 $\mu g\ m^{-3}$ for $PM_{10}$ and 25 $\mu g\ m^{-3}$ for $PM_{2.5}$ both on a daily average, and 9 ppm for CO on a 8-hour period average. Also shown is the correlation coefficient R between observations and model; the mean bias (MB) and the root mean square error (RMSE).*

| Variable | Station | Mean | | R | MB | RMSE | Number of excedances | |
|---|---|---|---|---|---|---|---|---|
| | | Obs. | Mod. | | | | Obs. | Mod. |
| $PM_{10}$ | Albion Park South | 27 | 42 | 0.78 | 28% | 40 | 2 | 4 |
| ($\mu$g m$^{-3}$) | Bargo | 73 | 36 | 0.21 | -29% | 109 | 3 | 3 |
| | Beresfield | 39 | 39 | 0.58 | -6% | 30 | 2 | 2 |
| | Bringelly | 33 | 41 | 0.61 | 18% | 27 | 2 | 4 |
| | Bulga | 41 | 40 | -0.05 | 2% | 36 | 2 | 5 |
| | Camden | 32 | 30 | 0.71 | -8% | 18 | 2 | 2 |
| | Campbelltown West | 32 | 26 | 0.83 | -21% | 16 | 1 | 2 |
| | Chullora | 31 | 33 | 0.58 | 5% | 22 | 2 | 4 |
| | Earlwood | 32 | 31 | 0.44 | -1% | 21 | 2 | 2 |
| | Kembla Grange | 37 | 50 | 0.91 | 6% | 43 | 4 | 5 |
| | Lindfield | 22 | 32 | 0.53 | 37% | 27 | 0 | 3 |
| | Liverpool | 34 | 37 | 0.85 | -1% | 17 | 2 | 5 |
| | Maison Dieu | 52 | 32 | -0.15 | -34% | 43 | 7 | 3 |
| | Mount Thorley | 52 | 34 | -0.23 | -19% | 40 | 7 | 4 |
| | Newcastle | 39 | 32 | 0.67 | -17% | 15 | 3 | 3 |
| | Oakdale | 36 | 35 | 0.83 | -9% | 19 | 4 | 3 |
| | Prospect | 34 | 46 | 0.84 | 16% | 32 | 1 | 5 |
| | Randwick | 29 | 25 | 0.48 | -10% | 14 | 1 | 1 |
| | Richmond | 44 | 75 | 0.68 | 50% | 64 | 5 | 5 |
| | Rozelle | 26 | 33 | 0.50 | 24% | 26 | 1 | 3 |
| | Singleton | 42 | 33 | -0.33 | -14% | 34 | 3 | 4 |
| | Singleton NW | 47 | 32 | -0.32 | -21% | 37 | 7 | 4 |
| | Singleton South | 39 | 32 | -0.41 | -5% | 36 | 2 | 3 |
| | St Marys | 35 | 47 | 0.82 | 20% | 29 | 2 | 5 |
| | Vineyard | 32 | 66 | 0.92 | 70% | 62 | 1 | 5 |
| | Wallsend | 31 | 34 | 0.55 | 14% | 16 | 1 | 3 |
| | Warkworth | 42 | 37 | -0.29 | -3% | 41 | 3 | 4 |
| | Wollongong | 38 | 38 | 0.79 | -1% | 21 | 3 | 3 |
| | **All** | **38** | **38** | **0.44** | **3%** | **33** | **75** | **99** |
| $PM_{2.5}$ | Beresfield | 19 | 31 | 0.25 | 73% | 31 | 1 | 5 |
| ($\mu$g m$^{-3}$) | Camden | 18 | 23 | 0.63 | 54% | 17 | 2 | 5 |
| | Chullora | 17 | 28 | 0.76 | 56% | 21 | 1 | 5 |
| | Earlwood | 14 | 25 | 0.54 | 82% | 21 | 1 | 4 |
| | Liverpool | 19 | 30 | 0.85 | 47% | 19 | 2 | 5 |
| | Richmond | 30 | 62 | 0.72 | 85% | 57 | 8 | 8 |
| | Singleton | 14 | 26 | 0.27 | 89% | 27 | 0 | 6 |
| | Wallsend | 20 | 26 | 0.46 | 60% | 17 | 3 | 5 |
| | Wollongong | 22 | 28 | 0.93 | 33% | 15 | 4 | 5 |
| | **All** | **19** | **31** | **0.60** | **64%** | **25** | **22** | **48** |
| CO | Camden | 251 | 207 | 0.79 | -6% | 132 | 0 | 0 |
| (ppb) | Campbelltown West | 511 | 203 | 0.86 | -58% | 402 | 0 | 0 |
| | Chullora | 307 | 285 | 0.72 | -4% | 93 | 0 | 0 |
| | Liverpool | 404 | 267 | 0.92 | -36% | 152 | 0 | 0 |
| | Newcastle | 202 | 207 | 0.49 | 8% | 83 | 0 | 0 |
| | Prospect | 237 | 306 | 0.92 | 24% | 116 | 0 | 0 |
| | Rozelle | 259 | 232 | 0.58 | -7% | 99 | 0 | 0 |
| | Wollongong | 473 | 267 | 0.99 | -35% | 386 | 0 | 0 |
| | Wollongong FTIR | 362 | 284 | 0.97 | -20% | 84 | 0 | 0 |
| | **All** | **330** | **247** | **0.79** | **-14%** | **183** | **0** | **0** |

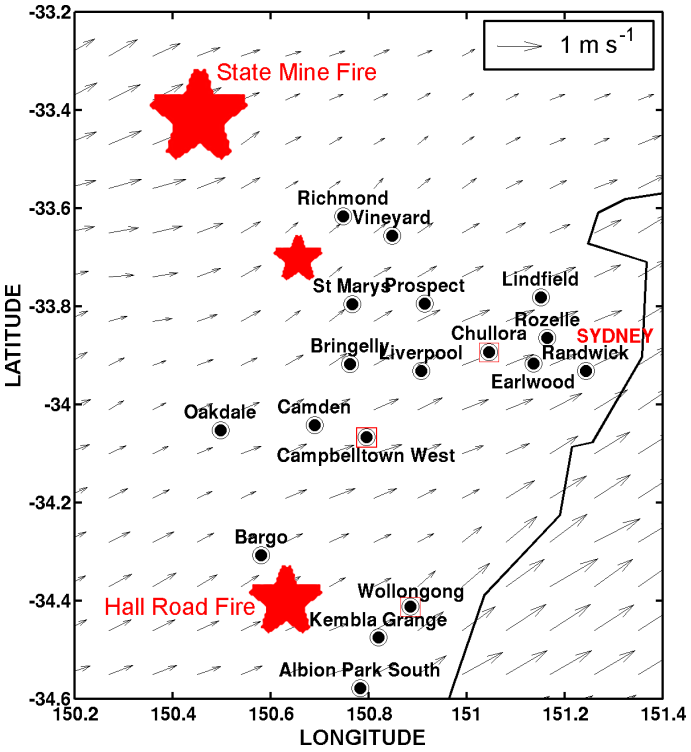


Figure 3: *Localization of OEH air quality monitoring stations in the Sydney area (source: Office of Environment and Heritage). The wind patterns (arrows) in October from the meteorological WRF model, as well as the major bushfire events (red stars) are also indicated.*

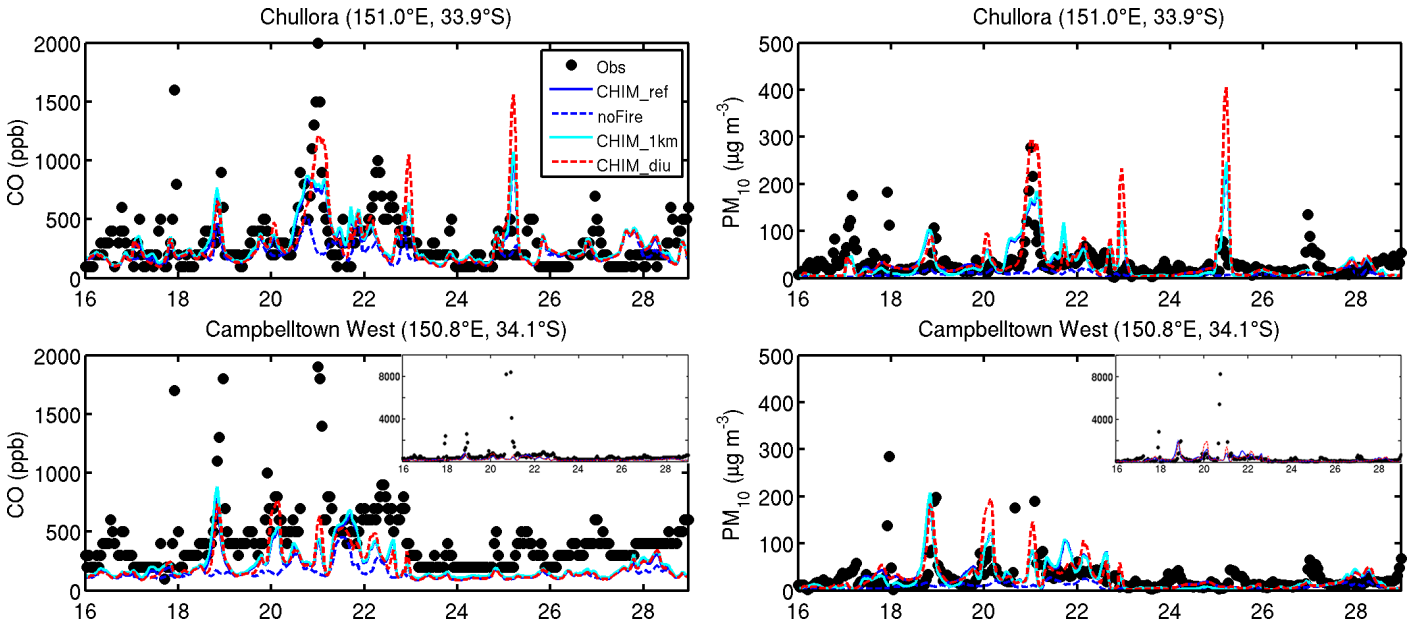


Figure 4: *Time series of CO and $PM_{10}$ surface concentrations for Chullora (Sydney east) and Campbelltown West and stations, for observations (black dots) and the CHIMERE model co-located (blue line). Results for two other CHIMERE simulations are also shown: in dashed blue, with all the fire emissions injected homogeneously under 1 km, and in dashed red with a diurnal profile for the amount of fire emissions. For Campbellown-West, time series with the y-axis going to 10 ppm for CO and 500 $\mu g\ m^{-3}$ is also shown to represent the concentration peak values.*

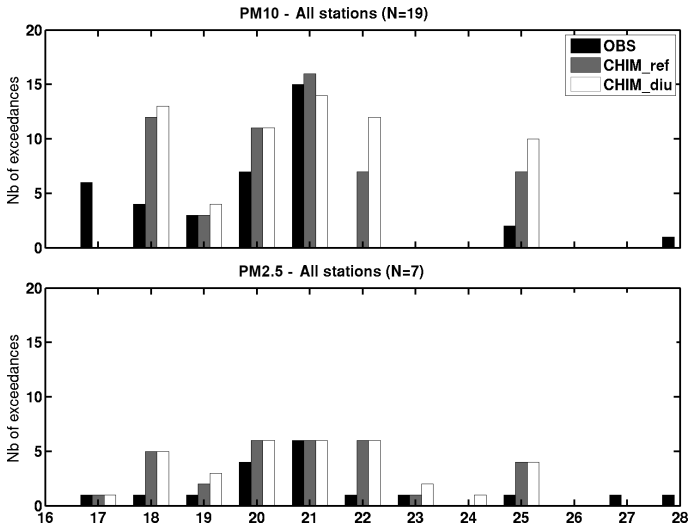


Figure 5: *Number of exceedances of the air quality standards (concentrations greater than 50 $\mu g\ m^{-3}$ for $PM_{10}$ and greater than 25 $\mu g\ m^{-3}$ for $PM_{2.5}$) depending on the day of October 2013. Black bars represents the exceedances detected in the observations, grey and white bars the one detected in the CHIM_ref (reference) and CHIM_diu (with a diurnal variability of fire emissions) simulations.*

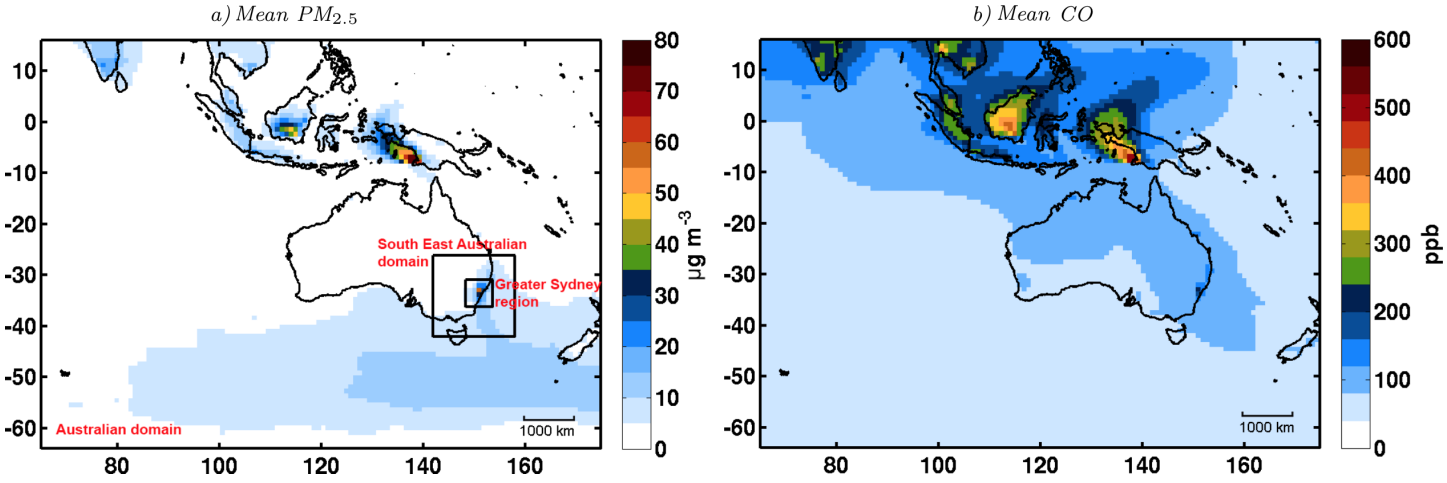


Figure 6: *a) Daily mean $PM_{2.5}$ and b) CO, averaged from 16 to 28 October 2013. Nested domains for the CHIMERE model are highlights with boxes on the top figure: the Australian domain, the South East Australian domain and the Greater Sydney Region.*

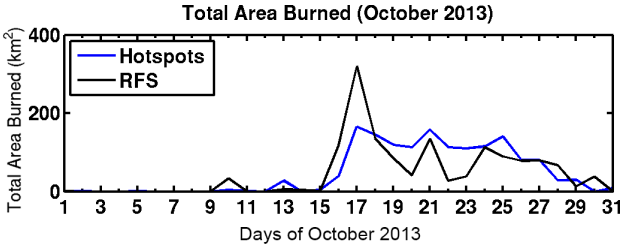


Figure 7: *Total area burned during NSW fires from 1 to 30 October 2013, reported by the Rural Fire Service (black line), and computed with the active fire products from MODIS (blue line).*

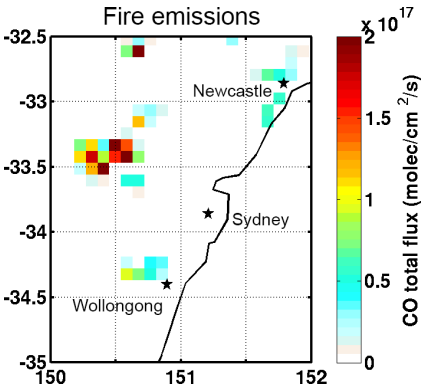


Figure 9: *Total fire emission flux of CO from 16 to 28 October 2013, calculated with the APIFLAME inventory.*

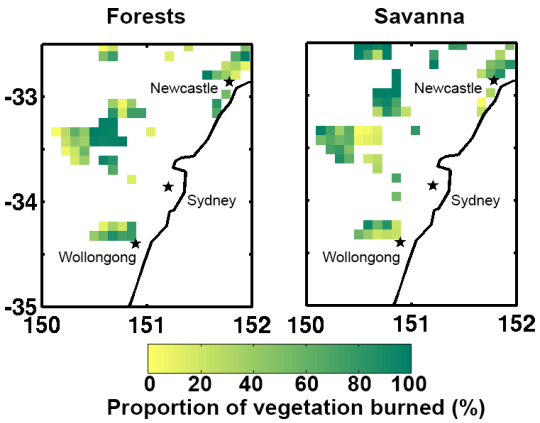


Figure 8: *Spatial partitioning of the proportion of vegetation burned during October 2013, according to the MODIS Vegetation Continuous Fields, for Forests and Savannas.*

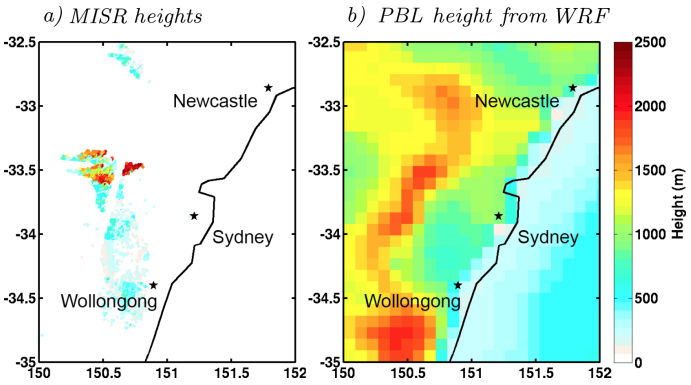


Figure 10: *a) Top heights of the fire plume on the 20th of October, as derived from measurements by the MISR instrument onboard the Terra satellite (Level 2 "TOA/Cloud heights and Winds" product). b) Modelled PBL height from WRF at the time of the MISR overpass.*

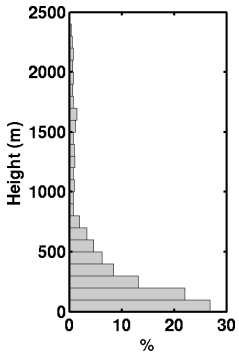


Figure 11: *Distribution of the heights seen by MISR on the 20th of October.*

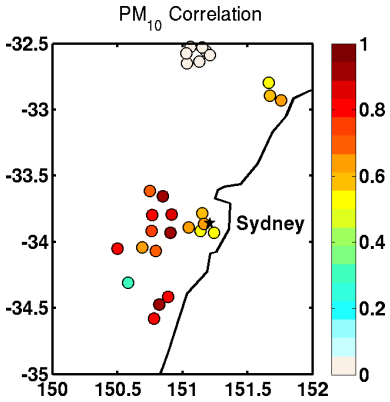


Figure 13: *Correlation between observed and modelled $PM_{10}$ concentrations from 16 to 28 October 2013 at the air quality monitoring stations.*

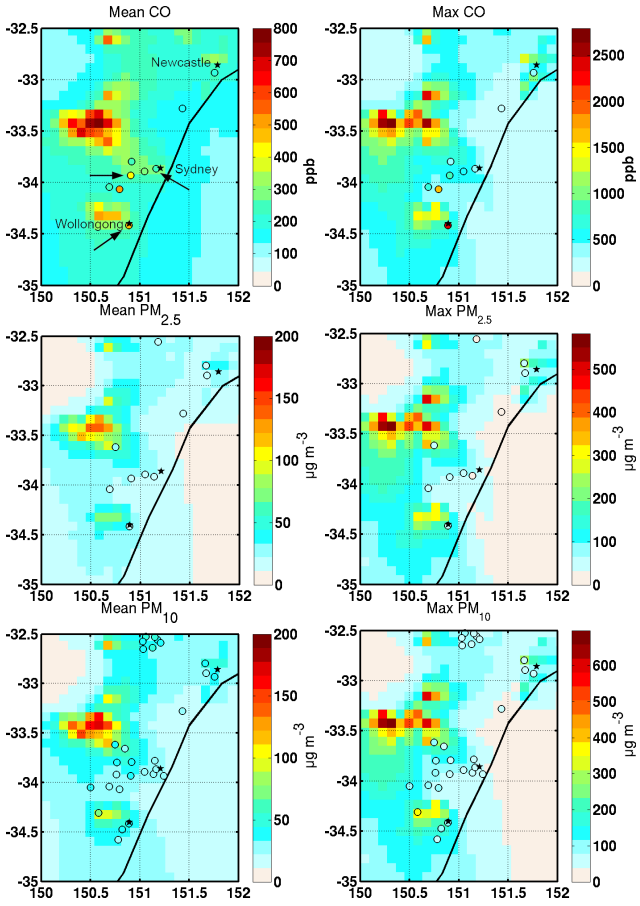


Figure 12: *Modelled daily mean and max of CO, $PM_{2.5}$ and $PM_{10}$, averaged over the fire event (16 to 28 October 2013). Observations from OEH stations are represented by the dots, arrows indicating the three stations that correspond to the plotted time series of Figures 2 and 4. The daily maximum is shown on the second column (with a different color scale).*

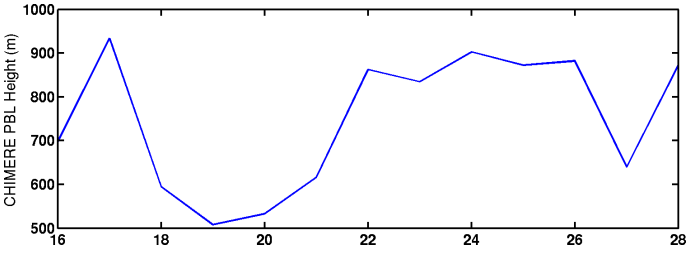


Figure 14: *Averaged simulated planetary boundary layer height above fires, from 16 to 28 October 2013.*

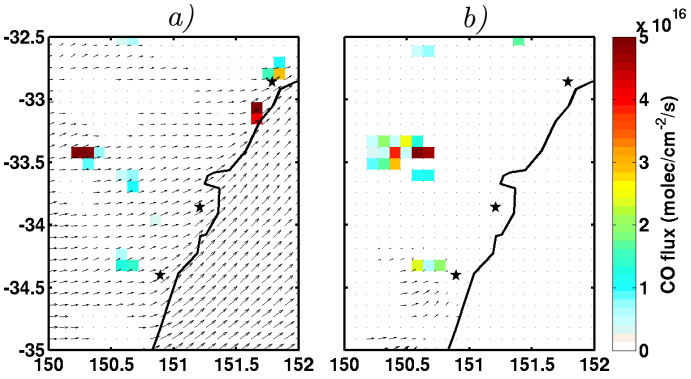


Figure 15: *Winds patterns for a) 17 October and b) 21 October from the model WRF. CO fluxes from the fire inventory are also plotted as an indicator of fire emissions.*